Bioconjugate Chemistry

Article

pubs.acs.org/bc

Fluorescence Enhancement upon G-Quadruplex Folding: Synthesis, Structure, and Biophysical Characterization of a Dansyl/Cyclodextrin-Tagged Thrombin Binding Aptamer

Stefano De Tito,[†] François Morvan,[‡] Albert Meyer,[‡] Jean-Jacques Vasseur,[‡] Annunziata Cummaro,[§] Luigi Petraccone,[§] Bruno Pagano,[†] Ettore Novellino,[†] Antonio Randazzo,[†] Concetta Giancola,[†] and Daniela Montesarchio*[,§]

[†]Department of Pharmacy, University of Naples Federico II, via D. Montesano 49, I-80131 Naples, Italy

[‡]Institut des Biomolécules Max Mousseron, UMR 5247 CNRS, Université Montpellier 1, Université Montpellier 2, Place E. Bataillon, 34095 Montpellier Cedex 5, France

[§]Department of Chemical Sciences, University of Naples Federico II, via Cintia 4, I-80126 Naples, Italy

Supporting Information

ABSTRACT: A novel fluorescent thrombin binding aptamer (TBA), conjugated with the environmentally sensitive dansyl probe at the 3′-end and a *β*-cyclodextrin residue at the 5′-end, has been efficiently synthesized exploiting Cu(I)-catalyzed azide−alkyne cycloaddition procedures. Its conformation and stability in solution have been studied by an integrated approach, combining in-depth NMR, CD, fluorescence, and DSC studies. ITC measurements have allowed us to analyze in detail its interaction with human thrombin. All the collected data show that this bis-conjugated aptamer fully retains its G-quadruplex formation ability and thrombin recognition properties, with the terminal appendages only marginally interfering with the conformational behavior of TBA. Folding of this modified aptamer into the chairlike, antiparallel G-quadruplex structure, promoted by K^+ and/or thrombin binding, typical of TBA, is associated with a net fluorescence enhancement, due to encapsulation of dansyl, attached at the 3′-end, into the apolar cavity of the *β*-cyclodextrin at the 5′-end. Overall, the structural characterization of this novel, bis-conjugated TBA fully demonstrates its potential as a diagnostic tool for thrombin recognition, also providing a useful basis for the design of suitable aptamer-based devices for theranostic applications, allowing simultaneously both detection and inhibition or modulation of the thrombin activity.

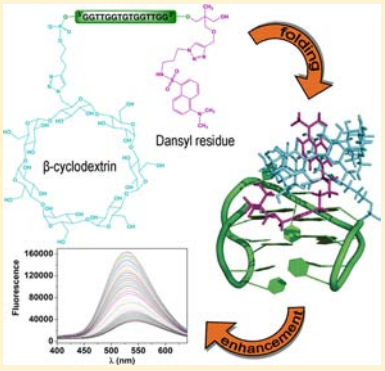

INTRODUCTION

Thrombin is a serine protease essential for homeostasis in many physiological systems,[1,2] playing crucial roles in the coagulation cascade, in which it converts soluble fibrinogen into insoluble fibrin and promotes a variety of different coagulation-related reactions.[3−5] For example, it is also involved in anticoagulation, fibrinolysis, tissue repair and wound healing, platelet and endothelial cell activation, progression of neoplasia, and inflammation, being dramatically dysregulated in patients affected by diseases such as lung cancer and diabetes mellitus, where its levels in plasma as free, unbound protein may be significantly higher than in healthy individuals.[6,7]

Thrombin inhibitors such as heparin, warfarin, and bivalirudin, commonly used as modulators of blood coagulation, typically produce severe side effects.[8−10] As a valid alternative to these classical inhibitors, several aptamers have been developed against thrombin, proving to be efficient anticoagulants, endowed with high affinity, nonimmunogenicity, and nontoxicity.[11,12] Two are the best studied aptamers for specific thrombin recognition: the so-called TBA_{15}, possessing 15 bases, and TBA_{29}, having 29 bases, that bind to exosite 1 and exosite 2, respectively, with dissociation constants (K_d) of about 100 and 0.5 nM.[13,14] TBA_{15}, which adopts a well characterized chairlike, antiparallel G-quadruplex structure, promoted by K^+ and/or thrombin binding, interacts with fibrinogen-binding exosite 1, thus inhibiting the thrombin-mediated coagulation.[15] Due to its intrinsic instability in physiological media, large amounts of it are needed to achieve effective anticoagulant responses. To overcome these drawbacks and obtain compounds with a proper pharmacokinetic profile, several modified TBA_{15} have been proposed,[16,17] incorporating modifications at the level of the nucleoside,[18−24] of the internucleoside linkages,[25−27] of the sequence,[28−30] as well as conjugation with PEG,[31] all employed to increase the target affinity or resistance against enzymatic hydrolysis.

The strong interest for TBA_{15} is motivated not only by its therapeutic potential, but also by its possible applications in biotechnological and analytical fields. In this context, a number

Received: July 29, 2013
Revised: October 2, 2013
Published: October 7, 2013

dx.doi.org/10.1021/bc400352s | *Bioconjugate Chem.* 2013, 24, 1917−1927

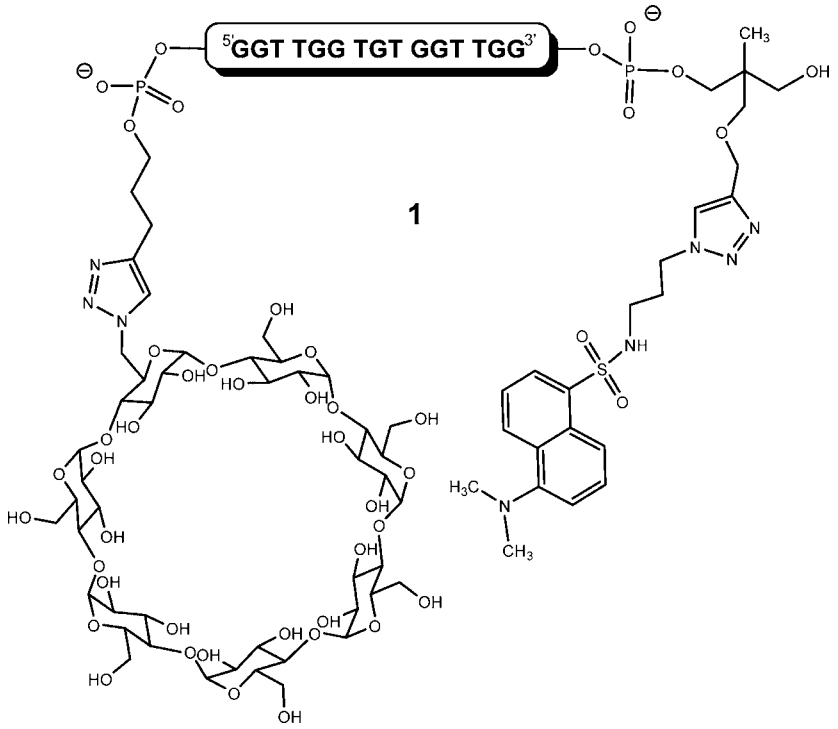

Figure 1. Bis-conjugated TBA_{15} **1** described in this study.

of TBAs incorporating fluorescent probes have been developed, to exploit the excellent sensitivity of fluorescence techniques for the detection of low levels of thrombin or potassium.[32−34] Typically, these fluorescent TBAs are among the most representative examples of aptamer beacons, i.e., oligonucleotides showing a net fluorescence decrease in response to folding processes. In these systems, TBAs are conjugated with a fluorescent probe and a quencher at their termini, which produce a fluorescence quenching if the oligonucleotide is folded in a G-quadruplex structure.[35,36] As an alternative approach, in a TBA bis-conjugated with pyrene, broad excimer emission is observed as a result of G-quadruplex formation, forcing the terminal pyrene moieties to spatial proximity.[37] In addition, fluorescent nucleosides can be incorporated at variable positions of the TBA sequence, producing different fluorescence changes,[38,39] and, remarkably, a biotinylated FRET probe based on a peptide-TBA conjugate—in association with streptavidin and a biotinylated nuclear export signal peptide—allowed to visualize K^+ concentration changes in HeLa cells.[40]

Aiming at combining in a unique molecular scaffold both the therapeutic and analytical potential of TBA_{15}, its labeling with fluorescent tags for turn-off/turn-on responses upon target recognition should be associated with chemical modifications in principle ensuring high *in vivo* stability and improved pharmacokinetic properties to the oligonucleotide. To the best of our knowledge, TBA-related aptamers designed to accomplish both these tasks are completely unprecedented in the literature.

Here we describe a modified TBA_{15}, conjugated with a dansyl group at the 3′- and a β-cyclodextrin residue at the 5′-end, showing a significant fluorescence change in the single strand → G-quadruplex conversion. Our design is based on the well-known inclusion properties of cyclodextrins, able to capture the environmentally sensitive dansyl probe, which in an apolar milieu exhibits a large fluorescence enhancement.[41]

The two terminal labels selected here, in principle allowing per se to increase the nuclease resistance of the G-rich oligonucleotide and improve its bioavailability, offer several additional advantages. Within the commonly used fluorescent dyes, the dansyl group is considered an excellent probe to study self-assembly or recognition processes, being dramatically sensitive to external stimuli. Typically, in different environments it exhibits large solvent-dependent fluorescence shifts and, among various applications, has been inserted in several potential drugs to investigate their mechanism of action, also allowing easy monitoring of their incorporation in cells.[42−44] As a further advantage, it is chemically stable and can be easily conjugated to systems containing primary amines or hydroxy functions starting from its commercially available chloride derivative. On the other hand, cyclodextrins are highly biocompatible, sugar-based macrocycles, able to encapsulate lipophilic agents and drugs in their internal, apolar cavity, whose use as molecular carriers is well documented in preclinical and clinical studies.[45,46] Sugars attached at the 5′-end of G-quadruplex structures have proved to tune the stability and properties of G-quadruplex structures.[47,48] Thus, cyclodextrins may profitably combine the desirable features of carbohydrates with the complexing ability of macrocycles.[49] For these reasons, the host−guest system dansyl-cyclodextrin has been selected to modify TBA_{15} so to render it suitable for potential applications directed at the diagnosis/therapy of coagulation-related disorders and/or other diseases in which high levels of circulating thrombin may occur.

Along with the synthesis, the detailed NMR analysis and DSC, CD, and fluorescence investigations on modified TBA_{15} **1** (Figure 1) are presented here, carried out to fully characterize its conformational properties in comparison with unmodified TBA_{15}, and, in parallel, ITC assays, performed to study its interaction with human thrombin.

Scheme 1. Synthesis of Bis-Conjugated TBA_{15} 1

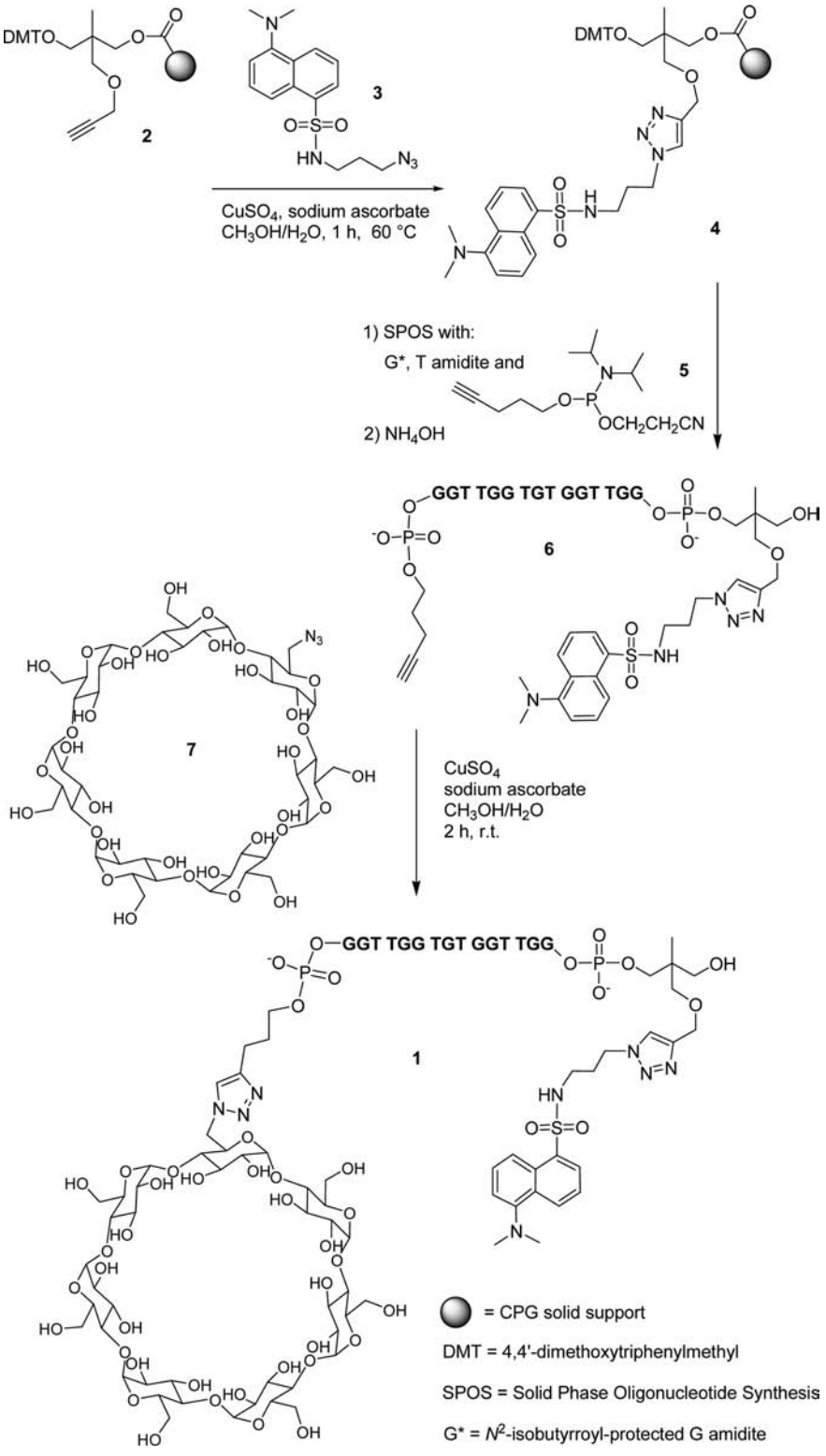

RESULTS AND DISCUSSION

Synthesis of Bis-Conjugated TBA_{15} 1. In our synthetic scheme, the bis-conjugated 15-mer **1** was synthesized in essentially three steps, as depicted in Scheme 1. First, dansyl azide derivative **3**[50] was immobilized by means of a Cu(I)-catalyzed azide−alkyne cycloaddition protocol[51,52] on alkyne-functionalized solid support **2**,[53] carried out using $CuSO_4$ and sodium ascorbate as catalysts for 1 h at 60 °C. On resulting functionalized solid support **4** the TBA_{15} sequence was assembled on a DNA synthesizer using standard phosphoramidite chemistry protocols (scale 1 μmol). The last coupling was performed with pent-4-ynyl phosphoramidite **5**[54] affording, after aq. ammonia treatment, the fully deprotected bis-conjugated oligonucleotide **6** in solution. Finally, β-cyclodextrin

dx.doi.org/10.1021/bc400352s | Bioconjugate Chem. 2013, 24, 1917−1927

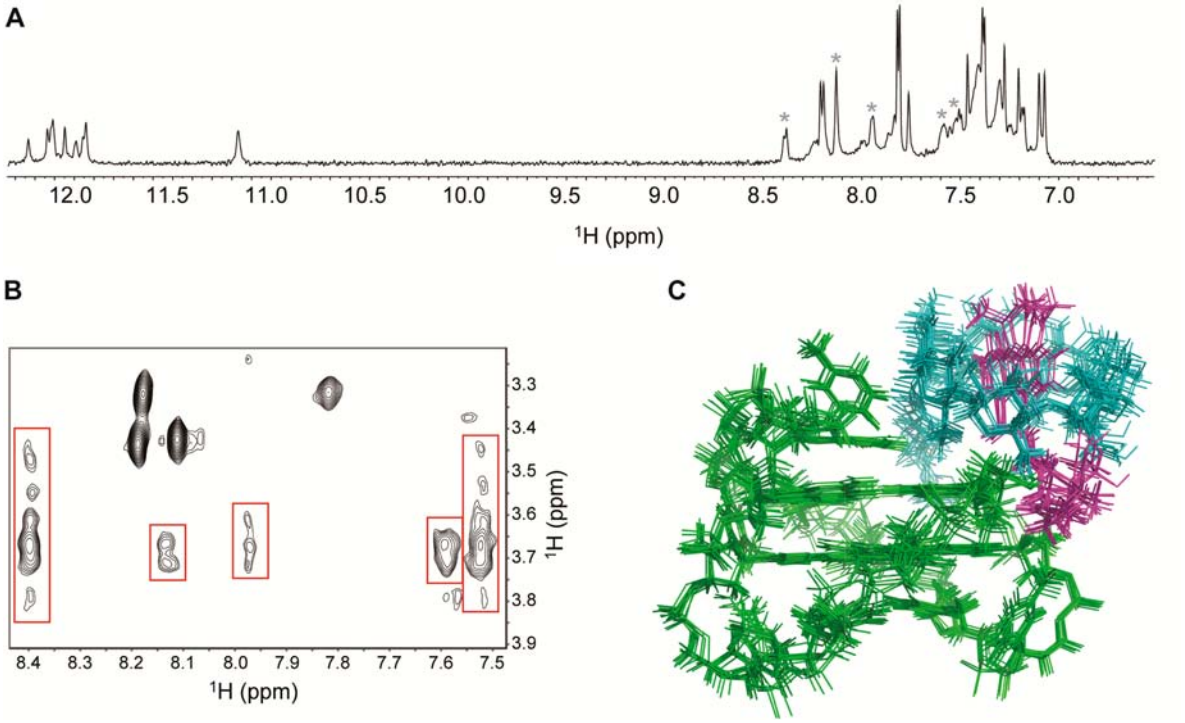

Figure 2. (A) Imino, amino, and aromatic regions of the 1D ^{1}H NMR spectra of **1** acquired at 25 °C (700 MHz). Signals marked by asterisks belong to the dansyl moiety. (B) Expanded region of the NOESY spectrum (700 MHz; T = 25 °C; m.t. 100 ms) of **1**. Cross-peaks between dansyl and β-cyclodextrin are red boxed. (C) Side view of the superimposition of the best 10 structures of **1**. DNA is reported in green, the β-cyclodextrin in cyan, and the dansyl moiety in magenta.

azide **7**, synthesized according to literature procedures,[55] was mixed with crude **6**, $CuSO_4$, and sodium ascorbate for 2 h at r.t., yielding target 5′-cyclodextrin, 3′-dansyl oligonucleotide **1**. After HPLC purification, **1** was isolated as a triethylammonium salt (4.0 mg) and characterized by MALDI-TOF mass spectrometry (see Figures S3 and S4, Supporting Information). Successively, to convert it into a potassium salt, **1** was left in contact with a 1 M KCl aq. solution at r.t. for 2 h. The resulting mixture was then concentrated and the buffer exchanged by Centricon centrifugation (Amicon Inc., Beverly, MA). The replacement of triethylammonium with potassium ions was confirmed by ^{1}H NMR spectra of **1**, showing the complete absence of resonances attributable to the triethylammonium spin system.

Nuclear Magnetic Resonance studies. The NMR sample of **1** was prepared at 1.0 mM concentration (0.6 mL, 90% H_2O/10% D_2O) in 10 mM KH_2PO_4 buffer containing 70 mM KCl, 0.2 mM EDTA (pH 7.0). The sample was heated for 10 min at 80 °C and slowly cooled down to room temperature, then the 1D ^{1}H NMR spectrum was recorded by using pulsed-field gradient sequence for H_2O suppression.[56,57]

Remarkably, the bis-conjugated TBA_{15} sequence was capable of forming a single well-defined hydrogen-bonded structure in solution, as clearly demonstrated by the presence of eight exchangeable proton signals in the region between 11.0 and 12.5 ppm of the spectrum (Figure 2A). These signals suggest the formation of a G-quadruplex structure involving Hoogsteen hydrogen bonds.[58] The nonexchangeable base and sugar protons of each deoxyribonucleotide unit of **1** were assigned through a combination of the analysis of 2D NOESY and 2D TOCSY (700 MHz, T = 25 °C) spectra (see Table S1 in the Supporting Information).

The 2D TOCSY experiment allowed us to assign almost all the proton resonances of each deoxyribose moiety. In particular, the assignments of the H2′/H2″ and H3′ resonances were easily accomplished detecting all the correlations with the H1′ protons, whose signals fall in an uncrowded spectral region. On the other hand, due to the very small coupling constant between H3′ and H4′, the assignment of the H4′ and H5′/H5″ resonances was realized also taking into account NOE connectivities. 2D NOESY experiments were used to determine the glycosidic angle conformations of each residue of the molecule and to assign the aromatic protons to the pertinent base, as well as to retrieve conformational information about the folding of **1**. Particularly, the presence of four intense cross-peaks between the H8 proton bases and sugar H1′ resonances, for residues G1, G5, G10, and G14, along with weak NOEs between the same aromatic protons and the H2′/H2″ of their own ribose moiety, indicated that these four residues adopt a *syn* glycosidic angle conformation. On the other hand, residues G2, G6, G8, G11, and G15 turned out to assume an *anti* glycosidic conformation, having opposite relative intensities of the afore-cited cross-peaks. Furthermore, the four H8 resonances of *syn* G residues are downfield shifted with respect to those of the *anti* ones, as also reported for TBA_{15}.[59] Interestingly, the NOESY spectrum showed that the four *anti*-Gs (G2, G6; G11, and G15) have classical H8/H2′−H2″ sequential connectivities to 5′ neighboring *syn*-Gs (G1, G5, G10, G14, respectively) allowing the assignment of the subunits G1−G2, G5−G6, G10−G11, G14−G15 (where the underlined residues adopt a *syn* glycosidic conformation). Moreover, the entire pattern of NOEs observed for the cited Gs indicates that the backbone conformations of these tracts resemble those of the unmodified TBA_{15} possessing a right-handed helix structure. In addition, the alternation of *syn* and

anti G residues implies that the studied oligonucleotide sequence folds into an antiparallel G-quadruplex structure, characterized by two G-tetrads, as in the case of unmodified TBA_{15}. Then, unusual NOE connectivities were observed between a number of Gs and Ts, indicating that $^{5'}TG^{3'}$ and $^{5'}GT^{3'}$ tracts do not adopt a helical winding, and that the TT and TGT tracts form loops. Therefore, the whole body of acquired data strongly indicates that the DNA backbone of **1** folds similarly to unmodified TBA_{15}, assuming a chairlike G-quadruplex structure. This is further inferred by the comparison of the NOE pattern of **1**, that closely resembles the one reported for unmodified TBA_{15}, thus indicating that the three-dimensional structures of the oligonucleotide portion of these compounds are almost superimposable.

Interestingly, the aromatic region of 1D ^1H spectrum of **1** shows six additional signals attributable to the dansyl moiety (δ_H 8.40, 8.13, 7.97, 7.59, 7.59, 7.52 ppm). The broadness of these signals suggested that the conformation of the dansyl group varies on a time scale close to the NMR one. The analysis of 2D TOCSY allowed us to assign the two spin systems of dansyl. Notably, each hydrogen of the dansyl moiety showed no connectivity with DNA protons, while a number of NOEs were detectable with protons resonating between 3.40 and 3.85 ppm (Figure 2B). This region of the spectrum is characteristic of the H3 and H5 protons of β-cyclodextrin. This result, also corroborated by fluorescence data, unambiguously demonstrates that the dansyl group is nicely encapsulated into the lipophilic cavity of β-cyclodextrin.

Restrained Structural Calculations. In order to obtain the three-dimensional structure of **1** at the atomic level, an estimation of proton−proton distances has been retrieved from cross-peak intensities in 2D NOESY experiments (700 MHz, T = 25 °C). A total of 303 distances were used for the calculations. All the distances have been clustered in three groups: strong NOEs ($1.0 < r_{ij} < 3.0$ Å), medium NOEs ($2.5 < r_{ij} < 4.5$ Å), and weak NOEs ($4.0 < r_{ij} < 6.0$ Å). Nevertheless, since the NOE cross-peaks between the β-cyclodextrin and the dansyl moieties were overlapped, the correct measurement of the volumes (distances) of the cross-peaks was not possible. For this reason we used constraints in the range $1 < r_{ij} < 6$ Å, that is the distance range in which NOEs are observable. Since the pattern of observed NOEs along the G1-G2, G5-G6, G10-G11, and G14-G15 tracts is typical of a B-DNA form, the backbone torsion angles α, β, γ, δ, and ε for those tracts were restrained in the ranges −150°/−30°, −230°/−110°, 20°/100°, 95°/175°, and −230°/−110°, respectively. Furthermore, glycosidic torsion angles χ were fixed in the *anti* domain (−155°/−75°) for G2, G6, G11, and G15, and in the *syn* domain (10°/90°) for G1, G4, G10, and G14.

Three-dimensional structures of **1** which satisfy NOEs were constructed by simulated annealing (SA) calculations. In order to eliminate any possible source of initial bias in the folding pathway, a starting structure of the oligonucleotide, characterized by an arbitrary conformation, was constructed and minimized. Restrained simulations were carried out for 275 ns using the CVFF force field as implemented in Discover software (Accelrys, SanDiego, USA). The starting point of restrained SA calculations was set at 1000 K, and, thereafter, the temperature was decreased stepwise down to 273 K. Then, the final step was to energy-minimize and refine the structures obtained by using the steepest descent followed by the quasi-Newton−Raphson (VA09A) algorithms. Twenty structures were generated. Average RMSD value of 0.55 ± 0.27 Å for all heavy atoms was obtained from the superimposition of the 10 best structures at lowest energy (Figure 2C). These data, along with the lack of significant violations of the experimental restraints, suggest that the obtained structures are representative of the structure effectively adopted in solution by **1**; its best computed conformation is represented in Figure 3. As

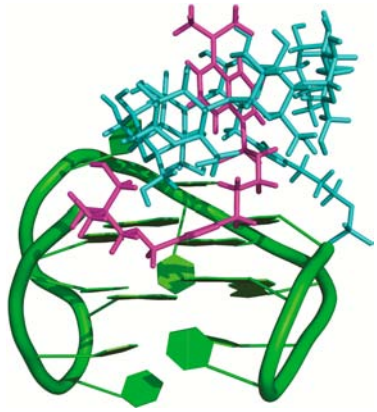

Figure 3. Best structure computed for **1**. DNA is reported in green ribbon. The β-cyclodextrin and the dansyl moieties are presented in cyan and magenta sticks, respectively.

expected, **1** exhibits a right handed helical backbone geometry and is characterized by the presence of three edge-wise connecting TT, TGT, and TT loops. As for unmodified TBA_{15}, **1** contains two stacked G-tetrads, with the same guanine *syn*/*anti* distribution around the G-tetrads, being characterized by the usual *syn*−*anti*−*syn*−*anti* and *anti*−*syn*−*anti*−*syn* arrangement of the two tetrads, respectively, and in the relative strand orientations, with two strands parallel to each other and two strands oriented in the opposite manner. In all 20 structures, as already highlighted by the presence of specific NOEs, the dansyl moiety conjugated at the 3′ extremity of **1** is caged into the lipophilic cavity of the β-cyclodextrin.

The lack of a perfect superimposition for the cyclodextrin/dansyl moieties in the superimposed structures (Figure 2C) indicates that this part of the molecule is able to adopt several stable conformations, suggesting a propensity for these groups to be flexible with respect to the DNA part of the molecule. Furthermore, the presence of the cyclodextrin/dansyl moieties does not bother the G-quadruplex structure and hence its stability, even if the loop TGT produces reduced stacking interactions with the external G-tetrad in comparison to unmodified TBA_{15}.

Stability and Fluorescence Properties of Bis-Conjugated TBA_{15} 1. The stability in solution of aptamer **1** was investigated by means of spectroscopic (CD, fluorescence) and calorimetric (DSC) techniques. The CD spectrum of the bis-conjugated TBA_{15} at 20 °C (Figure 4A) shows a negative band at 263 nm and two positive bands at 295 and 243 nm. These spectral characteristics are consistent with the reported CD spectrum of unmodified TBA_{15} forming an antiparallel G-quadruplex structure.[30,60−62] The CD melting profile monitored at 295 nm, shown in Figure 4B, is fully reversible, with no significant hysteresis observed between heating or cooling scans. van't Hoff analysis of the melting curve provided an enthalpy change of 135 kJ mol^{-1} and a melting temperature of 49 °C, values very close to the ones reported for unmodified TBA_{15}.[30,60−62] Next, the effect of the thermal unfolding on the

dx.doi.org/10.1021/bc400352s | *Bioconjugate Chem.* 2013, 24, 1917−1927

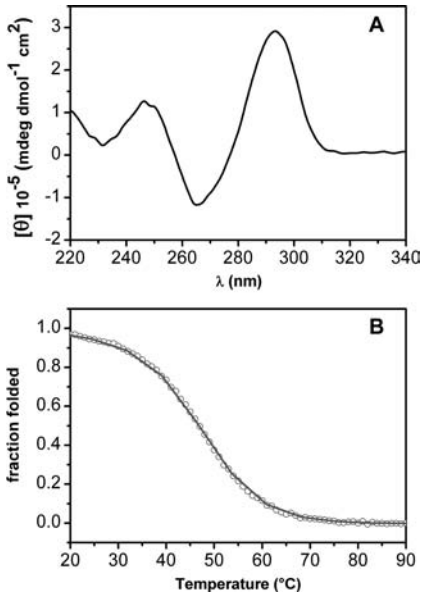

Figure 4. (A) CD spectrum at 20 °C of the bis-conjugated aptamer **1**. (B) CD melting profile of the bis-conjugated aptamer **1**. Fitting curve to a two-state denaturation process is also shown (continuous line).

fluorescence properties of aptamer **1** was explored by monitoring the fluorescence emission of the dansyl group on changing the temperature (Figure 5A). On increasing the

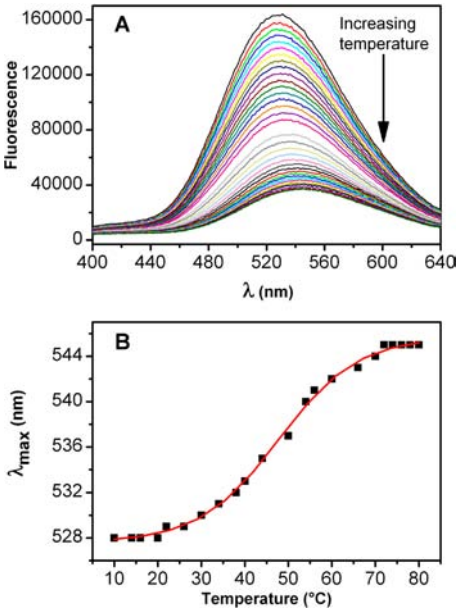

Figure 5. (A) Fluorescence spectra of the bis-conjugated aptamer **1** recorded on increasing the temperature in the range 10−80 °C. (B) Melting profile obtained by reporting the wavelength shift of the emission maximum as a function of temperature.

temperature, there is a gradual decrease in the fluorescence intensity up to ∼35 °C, followed by a sharp decrease in intensity in the 35−60 °C temperature range, and a further gradual decrease above 60 °C. In addition, the emission maximum shifts from 528 to 546 nm. These fluorescence changes clearly indicate that the dansyl group experiences dramatically different environments upon temperature-induced unfolding. These findings are consistent with the dansyl residue being encapsulated inside the β-cyclodextrin ring in the folded state (low temperature) and pointing outside, exposed to the solvent, in the unfolded state (high temperature). Figure 5B shows the melting curve obtained by reporting the wavelength shift of the emission maximum as a function of the temperature. The T_m (∼50 °C) is very close to the one obtained from the analysis of the CD-monitored melting curve (*cfr.* Figure 4B), suggesting that the dansyl group is thrown out from the cyclodextrin ring simultaneously with the unfolding of the whole G-quadruplex structure.

The thermodynamic stability of bis-conjugated aptamer **1** was further investigated by differential scanning calorimetry measurements.[63] The obtained DSC melting profile is shown in Figure 6. The reversibility of the DSC transition was confirmed

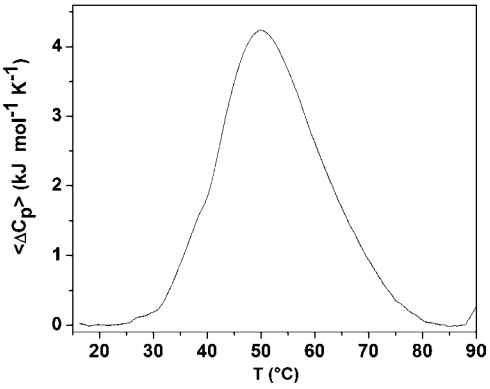

Figure 6. DSC profile of the bis-conjugated aptamer **1**, registered at 100 μM strand concentration and 1 °C/min scan rate.

by repeating several times the thermal scans on the same sample after cooling, which always yielded the same profile within experimental error. The maximum of the DSC profile is centered at 50 °C, showing a very good agreement between the DSC and CD-derived T_m values, also considering that the single strand concentrations used in the DSC experiments are approximately 20 times higher than those used in CD melting experiments. This agreement is a further confirmation that the bis-conjugated aptamer **1** folds into a unimolecular G-quadruplex structure. The integration of the denaturation peak gives a $\Delta H^\circ(T_m)$ of 102 kJ mol^{-1} and $\Delta S^\circ(T_m)$ of 0.31 kJ/(mol K). The enthalpy value derived from the DSC scan is lower than the one derived from the van't Hoff analysis of the CD melting curve, as already reported for unmodified TBA_{15}.[30] The calculated unfolding free energy at 37 °C was 5.9 kJ/mol, demonstrating that, at physiological temperature, bis-conjugated aptamer **1** forms a thermodynamically stable G-quadruplex.

All together, our spectroscopic and calorimetric data demonstrate that the structure adopted by aptamer **1** is thermodynamically stable under the studied experimental conditions. Furthermore, the fluorescence properties of aptamer **1** are fully consistent with the NMR structure showing the inclusion of the dansyl group in the β-cyclodextrin ring in the folded state.

Thrombin−Aptamer 1 Interaction. The ability of the bis-conjugated TBA_{15} **1** to bind to human thrombin was determined by isothermal titration calorimetry (ITC).[64] A representative ITC binding curve is shown in Figure 7A. ITC measurements revealed that aptamer **1** is able to bind human thrombin and that the interaction is an exothermic process. The

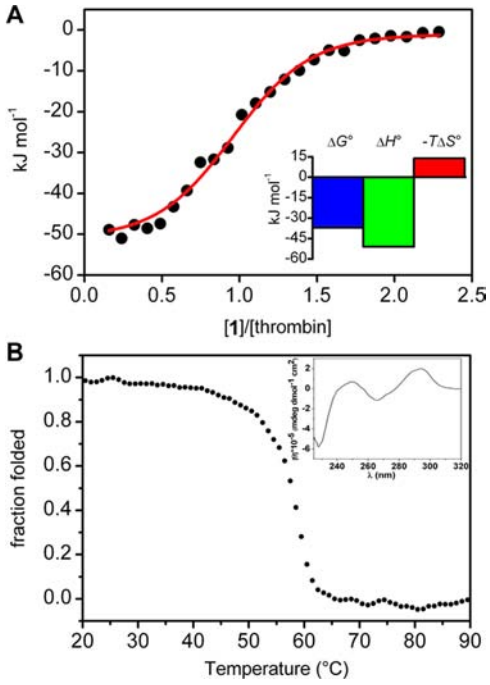

Figure 7. (A) ITC binding isotherm and thermodynamic signature (inset) for the interaction of bis-conjugated aptamer **1** with thrombin. (B) CD melting profile of the complex thrombin−aptamer **1** recorded at 295 nm. Inset: CD spectrum of the same sample at 20 °C.

plot of the integrated peaks as a function of the aptamer/protein molar ratio generated a curve with a sigmoidal shape, which was well fitted using an equivalent and independent binding sites model to give the stoichiometry and the equilibrium binding constant (K_b) of the interaction. The stoichiometry of the binding reaction was calculated to be 1, indicating a 1:1 aptamer/thrombin interaction. The K_b value was estimated to be 3×10^6 M^{-1} at 25 °C, a value comparable to some of the values previously reported for unmodified TBA_{15},[65] but slightly lower than others.[66,67] Nevertheless, the value of Gibbs free energy change derived ($\Delta_bG° = -37.2$ kJ mol^{-1}) indicates that the association is strongly favored from a thermodynamic point of view. Interestingly, Nallagatla et al. showed identical stoichiometry and comparable thrombin affinity for a TBA_{15} with 3′- and 5′-thymidine appendages.[20] The directly measured enthalpy change $\Delta_bH° = -51.0$ kJ mol^{-1} suggests the formation of favorable noncovalent interactions between bis-conjugated aptamer **1** and thrombin. Moreover, the thermodynamic signature of interaction (inset in Figure 7A) reveals that the binding is enthalpically driven, since the favorable enthalpic contribution exceeds the unfavorable entropy ($T\Delta_bS° = -13.8$ kJ mol^{-1}). Therefore, the thermodynamic data clearly demonstrate that the structural modifications introduced into aptamer **1** do not compromise the effectiveness of the interaction. Indeed, the slightly less favorable enthalpy measured for the interaction of thrombin with **1**—as in the case of unmodified TBA_{15} ($\Delta_bH°$ values reported in the literature range from −74 to −110 kJ mol^{-1})[65−67]—is compensated by a less adverse entropic contribution for the complex formation ($T\Delta_bS°$ values reported in the literature range from −30 to −72 kJ mol^{-1}).[65−67]

To evaluate the effect of the interaction with thrombin on the overall conformation and stability of aptamer **1**, CD experiments were carried out on aptamer **1** in mixture with human thrombin. Interestingly, as already shown in other cases,[68] the presence of the protein in the solution does not affect the CD spectrum of the G-quadruplex structure within the wavelength range 240−320 nm. In this range, the CD spectrum of the complex (inset of Figure 7B) retains the same shape (negative band at 263 nm and two positive bands at 295 and 243 nm) observed for free aptamer **1**, revealing no relevant changes in the G-quadruplex secondary structure of **1** upon binding with thrombin. Furthermore, when thrombin is added to the solution of **1**, the CD-monitored melting curve (Figure 7B) indicates a considerable increase in the thermal stability of the G-quadruplex ($\Delta T_m \sim +10$ °C), thus confirming the strong nature of the interaction.

CONCLUSION

A novel modified TBA_{15}, carrying a dansyl group and a β-cyclodextrin residue at its extremities, has been synthesized on a multimilligram scale, taking advantage of highly efficient Cu(I)-catalyzed azide−alkyne cycloaddition protocols. An in-depth NMR analysis of the bis-conjugated TBA_{15}, in association with CD, fluorescence, and DSC studies, showed that the dansyl probe can be efficiently lodged in the β-cyclodextrin cavity protruding from the folded oligonucleotide. Remarkably, the chair-type G-quadruplex structure of TBA_{15}, an essential motif for thrombin recognition, is neither sensibly distorted nor destabilized by the presence of the bulky conjugating agents. Thus, the transition from single strand to G-quadruplex produced a relevant fluorescence enhancement, as a result of the inclusion of dansyl into β-cyclodextrin, promoted by their spatial proximity in the G-quadruplex structure. ITC measurements allowed to analyze the thrombin recognition abilities of the bis-conjugated TBA_{15} and the comparison with previous data related to the unmodified aptamer proved that the tethers linked to the TBA_{15} sequence minimally affected its binding capability.

Taken together, the data presented here show bis-conjugated TBA_{15} **1** as a highly stable aptamer, easy to synthesize, and allowing a fully reversible fluorescence enhancement upon G-quadruplex folding, which therefore provides a sensitive and recyclable system for thrombin recognition without the addition of other reagents or oligonucleotide partners. This modified TBA_{15} offers a valuable and reliable model for the development of effective theranostic tools, envisaging innovative biomedical perspectives in the prevention and therapy of cardiovascular diseases. Our future efforts will be directed at (i) analyzing this aptamer in cell culture tests, and (ii) implementing this model system into suitable devices, to be used *in vivo* as potential therapeutic agents—allowing us to monitor the drug fate within cells—and/or *ex vivo* as fluorescent diagnostic tools, for early thrombin detection in biological fluids.

EXPERIMENTAL PROCEDURES

Synthesis of 5′-β-cyclodextrin-GGT TGG TGT GGT TGG-3′-dansyl 1. *Preparation of Dansyl-Modified Solid Support 4.* As described in Scheme 1, a 100 mM solution of dansyl propyl azide **3**[50] (54 μL, 9.0 μmol, 3 equiv) in CH_3OH, a freshly prepared 40 mM $CuSO_4$ solution (30 μL, 1.2 μmol, 0.4 equiv), and a 100 mM sodium ascorbate solution (60 μL, 6.0 μmol, 2 equiv) in water were added to the alkyne-functionalized Controlled Pore Glass (CPG) solid support **2**[53] (3 μmol) in a 1.2 mL solution of CH_3OH/water (1:1, v/v).

dx.doi.org/10.1021/bc400352s | *Bioconjugate Chem.* 2013, 24, 1917−1927

The vial containing the resulting mixture was sealed and placed in an oil bath for 60 min at 60 °C under a gentle magnetic stirring. Then, the CPG beads were filtered and washed with water (2 mL) and CH_3OH (2 mL) and then dried under reduced pressure.

Oligonucleotide Synthesis: 5′-Pent-4-ynyl-GGTTGGTGTGGTTGG-3′-{1-[2-methyl-2-(1-dansylprop-yl-1*H*-[1,2,3]triazol-4-yl-methoxymethyl)]propane-1,3-diol}. The dansyl-modified solid support **4** was dispatched into three columns onto which the synthesis of the sequence $^{5'}$GGTTGGTGTGGTTGG$^{3'}$ was carried out in parallel on an ABI 394 DNA synthesizer according to standard phosphoramidite chemistry protocols (1 μmol scale). Detritylation was performed with 2.5% dichloroacetic acid (DCA) in CH_2Cl_2 for 60 s. In the coupling step, 5-benzylmercapto-1*H*-tetrazole (0.3 M in anhydrous CH_3CN) was used as activator; commercially available 2′-deoxyribonucleoside phosphoramidites (0.09 M in anhydrous CH_3CN) were introduced with a 30 s coupling time and pent-4-ynyl phosphoramidite **5**[54] (0.2 M in anhydrous CH_3CN) was introduced with a 60 s coupling time. The capping step was performed with acetic anhydride using commercially available solutions (Cap A: acetic anhydride, pyridine, THF 10:10:80 v/v/v and Cap B: 10% N-methylimidazole in THF) for 10 s. Oxidation was performed with a standard, diluted iodine solution (0.1 M I_2, THF:pyridine:water 90:5:5, v/v/v) for 15 s.

General Procedure for Deprotection and Release in Solution of Oligonucleotide 6. The 15-mer functionalized CPG beads (3 × 1.0 μmol) were placed into a sealed vial and treated with concentrated aq. ammonia (1.5 mL) overnight at 55 °C. The supernatant was then withdrawn and concentrated under reduced pressure. The residue, containing 5′-pent-4-ynyl-oligonucleotide-3′-dansyl **6**, was redissolved in water for HPLC, MALDI-TOF (see Figures S1 and S2 in Supporting Information), and UV analyses (267 $OD_{260\ nm}$, 1.7 μmol, 56%) and successively used for the preparation of target **1**.

Conjugation of Oligonucleotide 6 with β-cyclodextrin Azide 7: Solution Procedure for the Cu(I)-Catalyzed 1,3-Dipolar Cycloaddition Reaction. A 57 mM solution of β-cyclodextrin azide **7**,[55] prepared as previously described (103 μL, 6 μmol, 3.5 equiv) in H_2O/DMSO (4:3, v/v), a freshly prepared 80 mM $CuSO_4$ solution (102 μL, 8.5 μmol, 5 equiv) and a 200 mM sodium ascorbate solution (204 μL, 43 μmol, 25 equiv) in water were added to 5′-pent-4-ynyl oligonucleotide-3′-dansyl **6** (1.7 μmol) in 400 μL of a CH_3OH/H_2O solution (1:1, v/v). The vial containing the resulting mixture was sealed and stirred at room temperature. After 2 h, the solution containing target oligonucleotide **1** was desalted by size exclusion chromatography on NAP 10 (GE Healthcare) according to the manufacturer's protocol and then purified by HPLC.

Analysis on HPLC Column. Macherey Nagel Nucleodur 100−3 C18 ec (75 mm × 4.6 mm). Solution A: 1% CH_3CN/0.05 M triethylammonium acetate (TEAAc), pH 7.0, Solution B: 80% CH_3CN/0.05 M TEAAc, pH 7.0. Gradient: 0% of B to 30% of B in A for 20 min. (Rt: 17.43 min).

Purification on HPLC Column. Macherey Nagel Nucleodur 100−7 C18 ec (125 mm × 8.0 mm). Gradient: 20% of B to 25% of B in A for 20 min. (Rt: 9.56 min) After purification, 4.0 mg of bis-conjugated oligomer **1** could be isolated (0.49 μmol, yield 29%), analyzed by HPLC and MALDI-TOF. MALDI-TOF *m/z*: $[M-H]^-$: for $C_{220}H_{294}N_{63}O_{138}P_{16}S$ calcd.: 6584.7, found: 6584.5.

Nuclear Magnetic Resonance Experiments. The NMR sample of bis-conjugate TBA **1** was prepared at ca. 1 mM concentration, in 0.6 mL (H_2O/D_2O 9:1, v/v) of a 10 mM KH_2PO_4, 70 mM KCl, 0.2 mM EDTA, pH 7.0 solution. NMR spectra were recorded with a Varian Unity INOVA 700 MHz spectrometer. ^{1}H chemical shifts were referenced relative to external sodium 2,2-dimethyl-2-silapentane-5-sulfonate (DSS). 1D proton spectra of samples in H_2O were recorded using pulsed-field gradient DPFGSE for H_2O suppression.[56,57] Phase-sensitive NOESY spectra[69] were recorded with mixing times of 100 and 200 ms (T = 25 °C). Pulsed-field gradient DPFGSE sequence was used for NOESY experiments in H_2O. TOCSY spectrum[70] was recorded with mixing times of 100 ms. All the experiments were recorded using STATES-TPPI procedure for quadrature detection.[71] In all 2D experiments, the time domain data consisted of 2048 complex points in t2 and 400−512 fids in t1 dimension. The relaxation delay was kept at 3 s for NOESY experiments used in the structure determination. A relaxation delay of 1.2 s was used for all the other experiments. The NMR data were processed on an Apple iMAC running iNMR (www.inmr.net).

Structure Calculations. Cross-peak volume integrations were performed with the program iNMR, using the NOESY experiment collected at mixing time of 100 ms. The NOE volumes were then converted to distance restraints after they were calibrated using known fixed distances of H2′/H2″ of G10 and G14. Then a NOE restraint file was generated with three distance classifications as follows: strong NOEs ($1.0 < r_{ij} < 3.0$ Å), medium NOEs ($2.5 < r_{ij} < 4.5$ Å), and weak NOEs ($4.0 < r_{ij} < 6.0$ Å). A total of 303 NOE derived distance restraints were used. Hydrogen bonds constraints were used ($1.7 < r_{ij} < 2.7$ Å). These constraints for H-bonds did not lead to an increase in residual constraints violation. A total of 32 backbone torsion angles were used in the calculations too. Particularly, the backbone torsion angles α, β, γ, δ, and ε were restrained in the range −150°/−30°, −230°/−110°, 20°/100°, 95°/175°, and −230°/−110°, respectively, and glycosidic torsion angles χ were fixed in the *anti* (−155°/−75°) and *syn* domains (10°/90°). The calculations have been performed using a distance dependent macroscopic dielectric constant of 4*r and an infinite cutoff for nonbonded interactions to partially compensate for the lack of the solvent used.[72] Thus the 3D structures which satisfy NOE and dihedral angle constraints were constructed by simulated annealing calculations. An initial structure of the oligonucleotide was built using a completely random array of atoms. Using the steepest descent followed by quasi-Newton−Raphson method (VA09A), the conformational energy was minimized. Restrained simulations were carried out for 275 ps using the CVFF force field as implemented in Discover software (Accelrys, San Diego, CA). The simulation started at 1000 K, and then the temperature was decreased stepwise until 273 K. The final step was again to energy-minimize in order to refine the obtained structures, using successively the steepest descent and the quasi-Newton−Raphson (VA09A) algorithms. Both dynamic and mechanic calculations were carried out by using 20 kcal mol^{-1} Å^{-2} flatwell distance restraints: 20 structures were generated. Root mean square deviation (RMSD) value of 0.55 ± 0.27 Å for heavy atoms was calculated for the 10 best structures. Illustrations of the structures were generated using the Pymol (PyMOL Molecular Graphics System, Version 1.2r3pre, Schrödinger, LLC.).

Circular Dichroism. Circular dichroism (CD) spectra and CD-monitored melting curves were recorded on a Jasco 715 circular dichroism spectrophotometer in a 0.1 or 1 cm path length cuvette and the wavelength was varied from 220 to 320 nm. The spectra were recorded with a response of 16 s at 2.0 nm bandwidth and normalized by subtraction of the background scan with buffer. The temperature was kept constant at 20 °C with a Jasco PTC-348 thermoelectrically controlled cell holder. The oligonucleotide concentration was 50 μM or 5 μM. CD-monitored melting curves were registered as a function of T from 20 to 90 °C at 295 nm with a scan rate of 1 °C min^{-1} and fitted by a two-state transition equation according to the van't Hoff analysis.[73] The melting temperature (T_m) and the enthalpy change ($\Delta H°$) values provide the best fit of the experimental melting data.

Differential Scanning Calorimetry. Differential scanning calorimetry (DSC) experiments were performed in a Nano DSC apparatus (TA Instruments, New Castle, DE, USA). All the solutions were prepared at 100 μM oligonucleotide concentration in a 10 mM potassium phosphate buffer, 70 mM KCl, 0.2 mM EDTA at pH 7.0. The excess molar heat capacity function ΔC_p was obtained after a baseline subtraction, assuming that the baseline is given by the linear temperature dependence of the native-state heat capacity. A buffer vs buffer scan was subtracted from each sample scan. The reversibility was checked by running the heating and cooling curves at the same scan rate of 1 °C/min. The transition enthalpies, $\Delta H°$, were obtained by integrating the area under the DSC curves. T_m is the temperature corresponding to the maximum of each DSC curve. Entropy changes were obtained by integrating the curve $\Delta C_p/T$ vs temperature. The thermodynamic parameters are the averages of values arising from three to five experiments. The errors on the parameters are standard deviations from the mean of multiple determinations.

Fluorescence Spectroscopy. Fluorescence spectra were collected in a 1 cm path length cuvette with a JASCO model FP-750 fluorometer equipped with a Peltier temperature controller. The oligonucleotide concentration was varied in the range 1−10 μM. The bis-conjugated oligonucleotide **1** was excited at 327 nm with a slit width of 5 nm, and emission spectra were collected from 400 to 600 nm over a range from 10 to 80 °C. Fluorescence melting curves were obtained by reporting the wavelength shift of the emission maximum as a function of temperature. The melting temperatures were determined from first derivative plots of the melting curves.

Isothermal Titration Calorimetry. Isothermal titration calorimetry (ITC) experiments were performed using a Nano ITC Low Volume from TA Instruments (Lindon, UT, USA) with a cell volume of 190 μL. Human thrombin (Sigma-Aldrich, Schnelldorf, Germany) and bis-conjugated TBA_{15} **1** samples were prepared in the same buffer. Titration experiments were carried out at 25 °C. Typically, 25 injections of 2 μL each of bis-conjugated TBA_{15} **1** solution (35 μM) were added to the thrombin solution (5 μM) every 300 s, with continuous stirring of the solution in the sample cell. Control experiments were carried out to calculate the heat of dilution for the bis-conjugated TBA_{15}. The corrected heat values were plotted as a function of the molar ratio to give the corresponding binding isotherm. The binding constant (K_b), enthalpy change ($\Delta_b H°$), and stoichiometry of the interaction process were obtained by fitting the binding isotherm to the equivalent and independent binding sites model, by using the NanoAnalyze software (TA Instruments). The remaining thermodynamic parameters of the interaction were calculated using the relationships:

$$\Delta_b G° = -RT\ln K_b$$

$$\Delta_b G° = \Delta_b H° - T\Delta_b S°$$

where $\Delta_b G°$ is the binding free-energy change, $\Delta_b H°$ is the binding enthalpy change, $\Delta_b S°$ is the binding entropy change, R is the gas constant (R = 8.314 J mol^{-1} K^{-1}), and T is the temperature in Kelvin (T = 298 K).

■ ASSOCIATED CONTENT

Supporting Information

HPLC and MALDI-TOF data for crude **6** and purified aptamer **1**. ^{1}H NMR assignments table of **1**. This material is available free of charge via the Internet at http://pubs.acs.org.

■ AUTHOR INFORMATION

Corresponding Author

*E-mail: daniela.montesarchio@unina.it. Tel.: +39-081-674126. Fax: +39-081-674393.

Notes

The authors declare no competing financial interest.

■ ACKNOWLEDGMENTS

We thank MIUR (PRIN 2009J54YAP_002 and 2009MFRKZ8_003) and Progetto FARO (Università di Napoli "Federico II", III tornata) for grants in support of this investigation. F.M. is member of INSERM.

■ REFERENCES

(1) Huntington, J. A. (2005) Molecular recognition mechanisms of thrombin. *J. Thromb. Haemostasis 3*, 1861-1872.
(2) Huntington, J. A., and Baglin, T. P. (2003) Targeting thrombin–rational drug design from natural mechanisms. *Trends Pharmacol. Sci. 24*, 589−595.
(3) Licari, L. G., and Kovacic, J. P. (2009) Thrombin physiology and pathophysiology. *J. Vet. Emerg. Crit. Care 19*, 11−22.
(4) Di Cera, E. (2008) Thrombin. *Mol. Aspects Med. 29*, 203−254.
(5) Wolberg, A. S. (2007) Thrombin generation and fibrin clot structure. *Blood Rev. 21*, 131−142.
(6) Pan, J., Qian, Y., Weiser, P., Zhou, X., Lu, H., Studelska, D. R., and Zhang, L. (2010) Glycosaminoglycans and activated contact system in cancer patient plasmas. *Prog. Mol. Biol. Transl. Sci. 93*, 473−495.
(7) Boden, G., Vaidyula, V. R., Homko, C., Cheung, P., and Rao, A. K. (2007) Circulating tissue factor procoagulant activity and thrombin generation in patients with type 2 diabetes: effects of insulin and glucose. *J. Clin. Endocrinol. Metab. 92*, 4352−4358.
(8) Hirsh, J. (2003) Current anticoagulant therapy–unmet clinical needs. *Thromb. Res. 109*, S1−S8.
(9) Warkentin, T. E., and Greinacher, A. (2003) Heparin-induced thrombocytopenia and cardiac surgery. *Ann. Thorac. Surg. 76*, 2121−2131.
(10) Rangarajan, S. (2011) Inhibitors of coagulation. *Haemophilia 17*, 90−94.
(11) Nimjee, S. M., Rusconi, C. P., Harrington, R. A., and Sullenger, B. A. (2005) The potential of aptamers as anticoagulants. *Trends Cardiovasc. Med. 15*, 41−45.
(12) Famulok, M. (2004) Turning aptamers into anticoagulants. *Nat. Biotechnol. 22*, 1373−1374.
(13) Bock, L. C., Griffin, L. C., Latham, J. A., Vermaas, E. H., and Toole, J. J. (1992) Selection of single-stranded DNA molecules that bind and inhibit human thrombin. *Nature 355*, 564−566.
(14) Padmanabhan, K., Padmanabhan, K. P., Ferrara, J. D., Sadler, J. E., and Tulinsky, A. (1993) The structure of alpha-thrombin inhibited

by a 15-mer single-stranded DNA aptamer. *J. Biol. Chem. 268*, 17651−17654.
(15) Macaya, R. F., Schultze, P., Smith, F. W., Roe, J. A., and Feigon, J. (1993) Thrombin-binding DNA aptamer forms a unimolecular quadruplex structure in solution. *Proc. Natl. Acad. Sci. U.S.A. 90*, 3745−3749.
(16) Aviñó, A., Fàbrega, C., Tintoré, M., and Eritja, R. (2012) Thrombin binding aptamer, more than a simple aptamer: chemically modified derivatives and biomedical applications. *Curr. Pharm. Des. 18*, 2036−2047.
(17) Musumeci, D., and Montesarchio, D. (2012) Polyvalent nucleic acid aptamers and modulation of their activity: a focus on the thrombin binding aptamer. *Pharmacol. Ther. 136*, 202−215.
(18) Borbone, N., Bucci, M., Oliviero, G., Morelli, E., Amato, J., D'Atri, V., D'Errico, S., Vellecco, V., Cirino, G., Piccialli, G., Fattorusso, C., Varra, M., Mayol, L., Persico, M., and Scuotto, M. (2012) Investigating the role of T7 and T12 residues on the biological properties of thrombin-binding aptamer: enhancement of anticoagulant activity by a single nucleobase modification. *J. Med. Chem. 55*, 10716−10728.
(19) Pasternak, A., Hernandez, F. J., Rasmussen, L. M., Vester, B., and Wengel, J. (2011) Improved thrombin binding aptamer by incorporation of a single unlocked nucleic acid monomer. *Nucleic Acids Res. 39*, 1155−1164.
(20) Nallagatla, S. R., Heuberger, B., Haque, A., and Switzer, C. (2009) Combinatorial synthesis of thrombin-binding aptamers containing iso-guanine. *J. Comb. Chem. 11*, 364−369.
(21) Raviv, S. M., Horvath, A., Aradi, J., Bagoly, Z., Fazakas, F., Batta, Z., Muszbek, L., and Harsfalvi, J. (2008) 4-thio-deoxyuridylate-modified thrombin aptamer and its inhibitory effect on fibrin clot formation, platelet aggregation and thrombus growth on subendothelial matrix. *J. Thromb. Haemostasis 6*, 1764−1771.
(22) Virno, A., Randazzo, A., Giancola, C., Bucci, M., Cirino, G., and Mayol, L. (2007) A novel thrombin binding aptamer containing a G-LNA residue. *Bioorg. Med. Chem. 15*, 5710−5718.
(23) Peng, C. G., and Damha, M. J. (2007) G-quadruplex induced stabilization by 2′-deoxy-2′-fluoro-D-arabinonucleic acids (2′F-ANA). *Nucleic Acids Res. 35*, 4977−4988.
(24) Saccà, B., Lacroix, L., and Mergny, J. L. (2005) The effect of chemical modifications on the thermal stability of different G-quadruplex-forming oligonucleotides. *Nucleic Acids Res. 33*, 1182−1192.
(25) Zaitseva, M., Kaluzhny, D., Shchyolkina, A., Borisova, O., Smirnov, I., and Pozmogova, G. (2010) Conformation and thermostability of oligonucleotide d(GGTTGGTGTGGTTGG) containing thiophosphoryl internucleotide bonds at different positions. *Biophys. Chem. 146*, 1−6.
(26) Martino, L., Virno, A., Randazzo, A., Virgilio, A., Esposito, V., Giancola, C., Bucci, M., Cirino, G., and Mayol, L. (2006) A new modified thrombin binding aptamer containing a 5′-5′ inversion of polarity site. *Nucleic Acids Res. 34*, 6653−6662.
(27) Russo Krauss, I., Merlino, A., Giancola, C., Randazzo, A., Mazzarella, L., and Sica, F. (2011) Thrombin-aptamer recognition: a revealed ambiguity. *Nucleic Acids Res. 39*, 7858−7867.
(28) Zhou, G., Huang, X., and Qu, Y. (2010) The binding effect of aptamers on thrombin. *Biochem. Eng. J. 52*, 117−122.
(29) Buff, M. C. R., Schafer, F., Wulffen, B., Muller, J., Potzsch, B., Heckel, A., and Mayer, G. (2010) Dependence of aptamer activity on opposed terminal extensions: improvement of light-regulation efficiency. *Nucleic Acids Res. 38*, 2111−2118.
(30) Smirnov, I., and Shafer, R. H. (2000) Effect of loop sequence and size on DNA aptamer stability. *Biochemistry 39*, 1462−1468.
(31) Dougan, H., Lyster, D. M., Vo, C. V., Stafford, A., Weitz, J. I., and Hobbs, J. B. (2000) Extending the lifetime of anticoagulant oligodeoxynucleotide aptamers in blood. *Nucl. Med. Biol. 27*, 289−297.
(32) Takenaka, S., and Juskowiak, B. (2011) Fluorescence detection of potassium ion using the G-quadruplex structure. *Anal. Sci. 27*, 1167−1172.
(33) Yang, H., Ji, J., Liu, Y., Kong, J., and Liu, B. (2009) An aptamer-based biosensor for sensitive thrombin detection. *Electrochem. Commun. 11*, 38−40.
(34) Lergaa, T. M., and O'Sullivan, C. K. (2008) Rapid determination of total hardness in water using fluorescent molecular aptamer beacon. *Anal. Chim. Acta 610*, 105−111.
(35) Li, J. J., Fang, X., and Tan, W. (2002) Molecular aptamer beacons for real-time protein recognition. *Biochem. Biophys. Res. Commun. 292*, 31−40.
(36) Wang, W., Chen, C., Qian, M. X., and Zhao, X. S. (2008) Aptamer biosensor for protein detection based on guanine-quenching. *Sens. Actuators, B 129*, 211−217.
(37) Nagatoishi, S., Nojima, T., Juskowiak, B., and Takenaka, S. (2005) A pyrene-labeled G-quadruplex oligonucleotide as a fluorescent probe for potassium ion detection in biological applications. *Angew. Chem., Int. Ed. 117*, 5195−5198.
(38) Johnson, J., Okyere, R., Joseph, A., Musier-Forsyth, K., and Kankia, B. (2013) Quadruplex formation as a molecular switch to turn on intrinsically fluorescent nucleotide analogs. *Nucleic Acids Res. 41*, 220−228.
(39) Musumeci, D., Oliviero, G., Roviello, G. N., Bucci, E. M., and Piccialli, G. (2012) G-quadruplex-forming oligonucleotide conjugated to magnetic nanoparticles: synthesis, characterization, and enzymatic stability assays. *Bioconjugate Chem. 23*, 382−391.
(40) Ohtsuka, K., Sato, S., Sato, Y., Sota, K., Ohzawa, S., Matsuda, T., Takemoto, K., Takamune, N., Juskowiak, B., Nagai, T., and Takenaka, S. (2012) Fluorescence imaging of potassium ions in living cells using a fluorescent probe based on a thrombin binding aptamer-peptide conjugate. *Chem. Commun. 48*, 4740−4742.
(41) Matsumura, S., Sakamoto, S., Ueno, A., and Mihara, H. (2000) Construction of alpha-helix peptides with beta-cyclodextrin and dansyl units and their conformational and molecular sensing properties. *Chem.—Eur. J. 6*, 1781−1788.
(42) You, L., and Gokel, G. W. (2008) Fluorescent, synthetic amphiphilic heptapeptide anion transporters: evidence for self-assembly and membrane localization in liposomes. *Chem.—Eur. J. 14*, 5861−5870.
(43) Leevy, W. M., Donato, G. M., Ferdani, R., Goldman, W. E., Schlesinger, P. H., and Gokel, G. (2002) Synthetic hydraphile channels of appropriate length kill Escherichia coli. *J. Am. Chem. Soc. 124*, 9022−9023.
(44) Coppola, C., Paciello, A., Mangiapia, G., Licen, S., Boccalon, M., De Napoli, L., Paduano, L., Tecilla, P., and Montesarchio, D. (2010) Design, synthesis and characterisation of a fluorescently labelled CyPLOS ionophore. *Chem.—Eur. J. 16*, 13757−13772.
(45) Stella, V. J., and He, Q. (2008) Cyclodextrins. *Toxicol. Pathol. 36*, 30−42.
(46) Loftsson, T., and Duchêne, D. (2007) Cyclodextrins and their pharmaceutical applications. *Int. J. Pharm. 329*, 1−11.
(47) Gómez-Pinto, I., Vengut-Climent, E., Lucas, R., Aviñó, A., Eritja, R., González, C., and Morales, J. C. (2013) Carbohydrate-DNA interactions at G-quadruplexes: folding and stability changes by attaching sugars at the 5′-end. *Chem.—Eur. J. 19*, 1920−1927.
(48) D'Onofrio, J., Petraccone, L., Martino, L., Di Fabio, G., Iadonisi, A., Balzarini, J., Giancola, C., and Montesarchio, D. (2008) Synthesis, biophysical characterization, and anti-HIV activity of glyco-conjugated G-quadruplex-forming oligonucleotides. *Bioconjugate Chem. 19*, 607−616.
(49) Szejtli, J. (1998) Introduction and general overview of cyclodextrin chemistry. *Chem. Rev. 98*, 1743−1753.
(50) Lewis, W. G., Magallon, F. G., Fokin, V. V., and Finn, M. G. (2004) Discovery and characterization of catalysts for azide-alkyne cycloaddition by fluorescence quenching. *J. Am. Chem. Soc. 126*, 9152−9153.
(51) Rostovtsev, V. V., Green, L. G., Fokin, V. V., and Sharpless, K. B. (2002) A stepwise Huisgen cycloaddition process: copper(I)-catalyzed regioselective "ligation" of azides and terminal alkynes. *Angew. Chem., Int. Ed. 41*, 2596−2599.

(52) Tornoe, C. W., Christensen, C., and Meldal, M. (2002) Peptidotriazoles on solid phase: [1,2,3]-triazoles by regiospecific copper(i)-catalyzed 1,3-dipolar cycloadditions of terminal alkynes to azides. *J. Org. Chem. 67*, 3057−3064.
(53) Lietard, J., Meyer, A., Vasseur, J. J., and Morvan, F. (2008) New strategies for cyclization and bicyclization of oligonucleotides by click chemistry assisted by microwaves. *J. Org. Chem. 73*, 191−200.
(54) Pourceau, G., Meyer, A., Vasseur, J. J., and Morvan, F. (2009) Azide solid support for 3′-conjugation of oligonucleotides and their circularization by click chemistry. *J. Org. Chem. 74*, 6837−6842.
(55) Tang, W., and Ng, S.-C. (2008) Facile synthesis of mono-6-amino-6-deoxy-alpha-, beta-, gamma-cyclodextrin hydrochlorides for molecular recognition, chiral separation and drug delivery. *Nat. Protoc. 3*, 691−697.
(56) Hwang, T. L., and Shaka, A. J. (1995) A modification of the excitation sculpting sequence. *J. Magn. Reson. A112*, 275−279.
(57) Dalvit, C. (1998) Efficient multiple-solvent suppression for the study of the interactions of organic solvents with biomolecules. *J. Biomol. NMR 11*, 437−444.
(58) Smith, F. W., and Feigon, J. (1992) Quadruplex structure of Oxytricha telomeric DNA oligonucleotides. *Nature 356*, 164−168.
(59) Schultze, P., Macaya, R. F., and Feigon, J. (1994) Three-dimensional solution structure of the thrombin-binding DNA aptamer d(GGTTGGTGTGGTTGG). *J. Mol. Biol. 235*, 1532−1547.
(60) Masiero, S., Trotta, R., Pieraccini, S., De Tito, S., Perone, R., Randazzo, A., and Spada, G. P. (2010) A non-empirical chromophoric interpretation of CD spectra of DNA G-quadruplex structures. *Org. Biomol. Chem. 8*, 2683−2692.
(61) Karsisiotis, A. I., Hessari, N. M., Novellino, E., Spada, G. P., Randazzo, A., and Webba da Silva, M. (2011) Topological characterization of nucleic acid G-quadruplexes by UV absorption and circular dichroism. *Angew. Chem., Int. Ed. Engl. 50*, 10645−10648.
(62) Randazzo, A., Spada, G. P., and Webba da Silva, M. (2013) Circular dichroism of quadruplex structures. *Top. Curr. Chem. 330*, 67−86.
(63) Pagano, B., Randazzo, A., Fotticchia, I., Novellino, E., Petraccone, L., and Giancola, C. (2013) Differential scanning calorimetry to investigate G-quadruplexes structural stability. *Methods 64*, 43−51.
(64) Pagano, B., Mattia, C. A., and Giancola, C. (2009) Applications of isothermal titration calorimetry in biophysical studies of G-quadruplexes. *Int. J. Mol. Sci. 10*, 2935−2957.
(65) Pagano, B., Martino, L., Randazzo, A., and Giancola, C. (2008) Stability and binding properties of a modified thrombin binding aptamer. *Biophys. J. 94*, 562−569.
(66) Nagatoishi, S., Isono, N., Tsumoto, K., and Sugimoto, N. (2011) Loop residues of thrombin-binding DNA aptamer impact G-quadruplex stability and thrombin binding. *Biochimie 93*, 1231−1238.
(67) Nagatoishi, S., Isono, N., Tsumoto, K., and Sugimoto, N. (2011) Hydration is required in DNA G-quadruplex-protein binding. *ChemBioChem 12*, 1822−1826.
(68) Cavaliere, P., Pagano, B., Granata, V., Prigent, S., Rezaei, H., Giancola, C., and Zagari, A. (2013) Cross-talk between prion protein and quadruplex-forming nucleic acids: a dynamic complex formation. *Nucleic Acids Res. 41*, 327−339.
(69) Jeener, J., Meier, B., Bachmann, H. P., and Ernst, R. R. (1979) Investigation of exchange processes by two- dimensional NMR spectroscopy. *J. Chem. Phys. 71*, 4546−4553.
(70) Braunschweiler, L., and Ernst, R. R. (1983) Coherence transfer by isotropic mixing: application to proton correlation spectroscopy. *J. Magn. Reson. 53*, 521−528.
(71) Marion, D., Ikura, M., Tschudin, R., and Bax, A. (1989) Rapid recording of 2D NMR spectra without phase cycling. Application to the study of hydrogen exchange in proteins. *J. Magn. Reson. 85*, 393−399.
(72) Weiner, S. J., Kollman, P. A., Case, D. A., Singh, U. C., Ghio, C., Alagona, G., Profeta, S., and Weimer, P. (1984) A new force field for molecular mechanical simulation of nucleic acids and proteins. *J. Am. Chem. Soc. 106*, 765−784.
(73) Marky, L. A., and Breslauer, K. J. (1987) Calculating thermodynamic data for transitions of any molecularity from equilibrium melting curves. *Biopolymers 26*, 1601−1620.